IOP Publishing J. Phys. Complex. 4 (2023) 025005 https://doi.org/10.1088/2632-072X/accc69

Journal of Physics: Complexity

OPEN ACCESS

RECEIVED
7 September 2022

REVISED
26 March 2023

ACCEPTED FOR PUBLICATION
12 April 2023

PUBLISHED
21 April 2023

PAPER

Effects of active noise on transition-path dynamics

Koushik Goswami[1] and **Ralf Metzler**[1,2,*]

[1] Institute of Physics & Astronomy, University of Potsdam, 14476 Potsdam-Golm, Germany
[2] Asia Pacific Centre for Theoretical Physics, Pohang 37673, Republic of Korea
[*] Author to whom any correspondence should be addressed.

E-mail: rmetzler@uni-potsdam.de

Keywords: barrier crossing, diffusion, transition path

Abstract

We propose an extension of the existing model describing a biomolecular reaction such as protein folding or ligand binding which is usually visualised as the barrier crossing of a diffusing particle in a double-well potential. In addition to the thermal noise, an active noise modelled in terms of an Ornstein–Uhlenbeck process is introduced to the dynamics. Within this framework, we investigate the transition-path properties of an underdamped particle surmounting an energy barrier, and we show explicitly how these properties are affected by the activity and persistence of the particle. Our theoretical study suggests that an active particle can cross the barrier at comparatively shorter timescales by lowering the (effective) barrier height. In particular, we study how the persistence time of the active force alters the transition-path time (TPT) at different friction limits. Interestingly, in one of our models we find a nonmonotonic behaviour of the TPT which is absent in the overdamped limit. The framework presented here can be useful in designing a reaction in a non-equilibrium environment, particularly inside a living biological cell in which active fluctuations keep the system out of equilibrium.

1. Introduction

A chemical reaction can be viewed as the exploration of a particle in a rough, multidimensional energy landscape [1–5]. However, to reduce the complexity of the problem, normally the collective features of the system are mapped onto a single, effective 'reaction coordinate' (RC) which becomes relevant in tracking the progress of the reaction [6–11]. In certain cases, the RCs have a direct physical meaning, e.g. the contour length of a polymer translocating through the nanopore [12], the geometric distance between two amino acids in internal protein dynamics [13, 14], or the gyration radius of small fluctuating proteins [15]. In the reduced space of the RC the stochastic dynamics is equivalent to the motion of a diffusing particle. Therefore, one can think of the reaction as the Kramers' escape problem in which the particle (or the RC) initially diffuses in a local minimum (reactant side) and then surmounts an energy barrier (ϵ) to reach the product side [1, 6]. The barrier height ϵ is estimated to be several times that of thermal energy $k_{\rm B}T$, $k_{\rm B}$ being the Boltzmann constant and T the reservoir temperature. So the particle spends most of the time near the minimum, attempting to cross the barrier, while only a few trajectories span across the barrier, leading to successful crossings towards the product side [16, 17]. Therefore, the time t_c of actual crossing is much shorter than the total reaction time τ_ε, which takes into account both kinds of quick successful crossing over the barrier and extended exploration on the reactant side [18–20]. From Kramers' theory the average of the total escape time can be expressed as $\langle\tau_\epsilon\rangle = A\exp(\epsilon/[k_{\rm B}T])$, where A is a prefactor, which depends on the mass of the particle, the shape of the barrier and the friction coefficient of the surroundings [1, 21].

A crucial step in decoding the cellular functioning is to know how biopolymers such as protein or nucleic acids and their assemblies fold into certain conformations. Owing to their complex nature, it poses a great challenge in understanding the entire process of folding [2, 4, 17, 22–24]. Like other simple biomolecular reactions, protein folding can also be assumed as a one-dimensional barrier crossing problem in a double-well potential with two minima corresponding to locally stable unfolded and folded conformations

of the protein [25–29]. Thus one considers only the 'relevant' degrees of freedom (typically, the RC) such as the distance between two probes on the protein chain, as it is usually done in experiments, to monitor the fluctuations of the distance and thereby providing information about the time scales associated with the reaction [13–15, 30–32]. To gain knowledge about the structural dynamics, one requires to unveil the shorter time scale t_c, namely, the duration of time the molecule takes just to successfully cross the barrier: this is the transition-path time (TPT), denoted here as $t_{\rm TP}$ [20, 33–35]. With the advancement of single-molecule measurements equipped with sufficient temporal resolution, it now becomes possible to obtain the TPT [18, 33, 34, 36–41], triggering a number of recent theoretical and simulations-based studies to corroborate experimental observations as well providing proposals for future directions [26–29, 35, 42–51].

As has been found experimentally, the dynamics of the RC can be described by a Markovian, simple diffusion process with an effective diffusion coefficient $D_{\rm eff}$, but the analysis using the same $D_{\rm eff}$ may lead to false predictions about other dynamical properties [52–54]. We note, however, that the appearance of longer-time Markovian kinetics may be substantially delayed, e.g. in internal protein dynamics [13, 14]. In many theoretical studies it is therefore suggested that the projection of the multidimensional landscape onto a single coordinate essentially introduces a memory effect [27–29, 35, 49, 55]. With this consideration, several theoretical models have been proposed, e.g. in some studies [27, 28, 55], the dynamics is modelled in terms of the generalised Langevin equation with a temporal memory kernel, taken as either power-law or exponential function. In [27], a correlated noise is included additionally to the system: this not only captures the effect of memory but also keeps the system out of equilibrium. Such a noise is often referred to as active noise, which may stem from some active processes such as ATP hydrolysis [56–61]. In fact, a process driven by an active force is ubiquitous in biological systems—examples of such realisations include, i.a., self propulsion of bacteria, motility of cells, and movement of motor proteins along the filaments inside a living cell [62–68]. Other examples in which active forces play an important role are the assisted looping kinetics of a polymer in a bath of self-propelled particles or random fluctuations of chromosomal loci driven by enzymatic activity, etc [69, 70]. An energetic cost is involved in these processes, resulting in broken detailed balance [60, 71–73]. It is worth noting here that to date most experiments on protein folding have been performed in an equilibrium set-up [74]. However, at non-equilibrium conditions, e.g. for chaperone-assisted protein folding inside the cellular environment, or in an actively swirled, highly crowded cellular cytoplasm [75], the reaction is found to be faster compared to its equilibrium counterpart [76, 77]. Another related problem is the translocation (as well as the folding) of an active polymers through a pore which too can be conceived as a diffusive motion over a barrier where the contour length of the translocating polymer is considered as the RC [78]. The study of active polymer turns out to be of great importance for the characterisation of a biopolymer as recent observations on genomic mobility revealed the presence of an active force along its backbone [79, 80]. Apart from the activity arising from an intrinsic source as in the case of an active polymer, the experiment can be performed on a passive system with the application of an external force which mimics an active noise, as discussed below.

Although the effect of active forces on the transition-path has been addressed earlier, e.g. in the context of protein folding, see [27], the contribution of inertia was mostly ignored by considering the overdamped limit. In the presence of memory, it is found to be important to incorporate the inertial effect into the Langevin dynamics to predict the accurate rate for the reduced description of a reaction [81]. The (effective) mass involving in such dynamics can be estimated by application of the equipartition theorem on the velocity data extracted from trajectories. In a simulation study on the dissociation of NaCl in water, the increase in transition-path probability by up to 40%–50% has been observed due to inertial effects [82]. Thus it is of interest to investigate the role of underdamped dynamics as well as the active force individually for such shorter segments of trajectories. This study may also be applicable to a generic biomolecular reactions occurring in a low-density medium [83, 84], or for a rearrangement and isomerisation reaction involving rotational dynamics, for which inertia plays an important role on the speed of the reaction [85, 86]. Its applicability can be extended to the target search (TS) problem for active particles, a topic with great relevance in biology—whether it is a bacteria searching for nutrients or a protein locating a promoter site on the DNA chain to initiate the transcription [87, 88], it can be mapped onto a TS problem. But only a few studies have considered a TS problem where the reactant is driven by both thermal and active force, particularly in the underdamped limit, and the target site and the reactant site are separated by a high energy barrier [89–93]. In a recent experiment [94], Militaru *et al* investigated the activated escape of a nanoparticle trapped inside a double-well potential in both high and low friction limits. They generated the active noise by applying an electrostatic force externally which induces self-propulsion of the particle. Their key finding is a non-monotonic variation of the transition rate as a function of its rotational diffusivity ($D_{\rm R}$). For lower values of the rotational diffusivity, i.e. for a highly correlated motion, the rate is reduced with decreasing $D_{\rm R}$. Specifically, in the high $D_{\rm R}$ limit, the enhancement of the rate was clearly observed with the decrease of $D_{\rm R}$, evincing an activity-assisted escape over a lower effective barrier.

Motivated by the above examples, we here consider the barrier crossing event of an underdamped active particle in one dimension. The particle is initially confined in the left well of a double-well potential, and it is attempting to overcome the barrier to reach the right well, which can be thought of as a target or product side. As mentioned above, an active force acting on the particle can be realised in two ways: (i) athermal fluctuations arising from an internal mechanism as in the case of an active polymer [79] or (ii) an external stochastic force generated from a driven crowded environment [75] or a custom-programmed input as employed in [94]. But we do not distinguish the two cases as the noises with same statistical properties have similar effects on the dynamics, at least on the single-particle level. Here our aim is to find analytically the transition-time distribution and TPT of the above system. We further analyse the effects of activity, persistence and friction coefficient of the bath on the transition properties.

2. Model

We consider a particle of mass m performing a random motion in a one-dimensional double-well potential $V(x)$ at ambient temperature T. Along with the thermal noise $\eta(t)$ from the reservoir, the particle is subjected to an additional noise $\sigma(t)$ which may refer to the self-propulsive force of a self-propelled particle, the noise arising from a chemical reaction to aid the directed walk of a motor protein, or the driving by active particles in the surrounding. There is no dissipative term corresponding to the fluctuations described by $\sigma(t)$, implying that the system is driven out of equilibrium [72, 73, 95]. At $t = 0$, the particle is in the left well of the potential, and so one can assume that it already achieves a local steady state inside the well before it crosses the barrier. Now the stochastic equation describing the particle's dynamics is given by [96–98]

$$m\ddot{x}(t) + m\gamma\dot{x}(t) = -V'(x) + \eta(t) + \sigma(t), \tag{1}$$

where γ is the drag coefficient of the bath, and it is related to the thermal diffusivity D_{T} via the Einstein–Smoluchowski–Sutherland relation $k_{\mathrm{B}}T = m\gamma D_{\mathrm{T}}$. We note that the mass m here is an effective measure, and we will show that it effects modifications in the reduced description of the active process, similar to observations in [81]. As usual, $\eta(t)$ is a zero-mean white Gaussian noise, which follows the fluctuation-dissipation theorem (FDT), $\langle\eta(t_1)\eta(t_2)\rangle = 2m\gamma k_{\mathrm{B}}T\delta(t_1 - t_2)$. Moreover, the active noise $\sigma(t)$ violates the FDT, and as a simple model, the time evolution of $\sigma(t)$ is described by the Ornstein–Uhlenbeck process (OUP) [57, 60, 71]

$$\dot{\sigma}(t) = -\frac{1}{\tau_A}\sigma(t) + \frac{1}{\tau_A}\eta_A(t) \tag{2}$$

where η_A is a zero-mean, delta-correlated Gaussian noise with the noise strength ${\sigma_0}^2$. The active OUP noise $\sigma(t)$ is an exponentially correlated noise with autocorrelation function [99]

$$\langle\sigma(t_1)\sigma(t_2)\rangle = \frac{\sigma_0^2}{\tau_A}\exp\left(-\frac{|t_1 - t_2|}{\tau_A}\right), \tag{3}$$

where τ_A is the persistence time of the noise. This model is usually used to describe the dynamics of a passive tracer in a low-density active bath where the pronounced enhancement of the tracer's diffusivity has been observed [57, 100]. A similar model for $\sigma(t)$ is the modified Ornstein–Uhlenbeck process (MOUP) which can be realised by the following stochastic equation:

$$\dot{\sigma}(t) = -\frac{1}{\tau_A}\sigma(t) + \frac{1}{\sqrt{\tau_A}}\eta_A(t). \tag{4}$$

So the correlation for the MOUP model can be expressed as

$$\langle\sigma(t_1)\sigma(t_2)\rangle = \sigma_m^2\exp\left(-\frac{|t_1 - t_2|}{\tau_A}\right), \tag{5}$$

which has a similar form as the OUP case, but here the amplitude of the correlation does not depend on the persistence time τ_A. Thus both models can be mapped onto each other just by replacing σ_0^2/τ_A in (3) with a term σ_m^2 to obtain equation (5). For a self-propelled particle, $\sigma(t)$ corresponds to its velocity with a fixed average speed σ_m, and the motion persists in a particular direction over an average time period τ_A [98]. Note that the dynamical behaviour, which remains within the Gaussian domain, is well captured by the above models. For more information, we refer to [97, 98]. Analogous to the MOUP case, the telegraphic noise can also be characterised by an exponential correlation function, and it is often invoked to describe processes within the cellular environment where the distribution deviates from Gaussian statistics [61, 101]. For

example, motor proteins exert an active force on a tracer immersed in the cytosol by creating pulses at random intervals sampled from a Poisson distribution with an average waiting time τ_w [61, 72]. If the value of τ_w is comparatively small, one can assume the deviations from Gaussianity to be negligible. Then the above case can reasonably be approximated by the MOUP. Another non-Gaussian model is described by an active Brownian particle (ABP) where the particle under a fixed amplitude of force changes its direction stochastically due to its rotational diffusion [94]. This means that the rotational diffusivity (D_R) is inversely related to the persistence time τ_A, *i.e.*, $D_R = \tau_A^{-1}$. Again, this model is associated with a similar correlation function as the one in (5). Thus the MOUP description represents a Gaussian approximation of the ABP model which allows analytical predictions.

To specify transition paths, it is necessary to assign one entry point on the left side of the potential and one exit point on the right for the transition-path trajectories at which the absorbing boundary conditions should be posed. For the sake of simplicity, the position of the barrier top is taken to be $x = 0$, and the entry and exit points are at $-x_c$ and $+x_c(>0)$, respectively. Since only a portion around the barrier top is required to find transition-paths, one can approximate $V(x)$ as an inverted parabolic potential of the form: $V(x) \approx -\frac{1}{2}\kappa_b x^2$, where κ_b is the stiffness of the potential corresponding to the barrier top. Therefore from equation (1) the dynamics of the particle around the barrier top $x = 0$ can be rewritten as

$$\frac{1}{\gamma}\ddot{x}(t) + \dot{x}(t) = \frac{\kappa_b}{m\gamma}x(t) + \eta(t) + \sigma(t). \tag{6}$$

Here we rescaled all terms by $m\gamma$, such that (3) turns into $\langle\sigma(t_1)\sigma(t_2)\rangle = (D_A/\tau_A)\exp(-|t_1 - t_2|/\tau_A)$, where now $D_A = \sigma_0^2/(m^2\gamma^2)$ is the active diffusivity stemming from the active noise. Similarly from (5) one can write the strength of the noise–noise correlation as $C_A = (\sigma_m/[m\gamma])^2$, which basically represents the square of the 'swim speed' when $\sigma(t)$ is used to model the self propulsion of a self-propelled particle. For the sake of notational brevity, we keep the same symbols in equation (6) to denote the rescaled variables. Note that in the OUP-noise case $\sigma(t)$ becomes delta-correlated in the limit $\tau_A \to 0$, and thus it behaves like a thermal noise. It implies that the motion can then be characterised by an effective diffusivity $D_{\rm eff} = D_T + D_A$. Unless mentioned otherwise we mostly analyse our results based on the OUP noise. Notice that finding a theoretical expression of the probability density function (PDF) with the absorbing boundary conditions mentioned above is often a difficult task. However, we can easily derive the PDF using the free boundary conditions as discussed in appendix A. Following the previous studies [27, 35, 102, 103], one can simply use the PDF of the free case to obtain the transition-path properties, provided that barrier (ΔV) is high enough for purely thermal escape, i.e. $\epsilon_p = (\kappa_b x_c^2)/(2k_BT) \gg 1$. It is worthwhile noting here that the experiments on transition paths are usually performed implying absorbing boundary conditions, i.e. once a trajectory crosses the exit point for the first time before it reverts back to the entry point, it is discarded and is regarded as a successful transition. From a theoretical point of view, it can be properly implemented if the re-crossing events around the exit point are minimised. As the normal mode transformation theory by Pollak suggests [35], such events become least probable in the limit $(\Delta V)/(k_BT) \gg 1$. Therefore, our following analysis is based on the free boundary condition in the sense of the above approximation.

3. Transition-path properties

We now discuss the transition-path properties for transition-paths in the region $x \in [-x_c, +x_c]$. The number of trajectories in this region with TPTs shorter than t can be estimated in terms of the absorption function $Q_c(t, x_c)$, which is actually related to the survival probability $\mathscr{S}(t, x_c)$ as $Q_c(t, x_c) = 1 - \mathscr{S}(t, x_c)$, is defined as [26]

$$Q_c(t, x_c) = \int_{x_c}^{\infty} {\rm d}x_t P(x_t, t|-x_c, 0). \tag{7}$$

In principle, $P(x_t, t|-x_c, 0)$ is the PDF to find the process at RC x_t at time t after release at $x_0 = -x_c$ at $t = 0$ with absorbing boundary conditions at $x = -x_c$ and $x = +x_c$. But as already mentioned, a good approximation is the PDF with free boundary conditions as given by (A.11), taking into account the fact that $\kappa_b x_c^2 \gg k_BT$. Using equation (A.11) one can compute the absorption function

$$Q_c(t, x_c) = \int_{x_c}^{\infty} {\rm d}x_t P(x_t, t|-x_c, 0) = \frac{1}{2}{\rm erfc}(q(t)). \tag{8}$$

Here we defined (for the full expression for ϕ see appendix A)

$$q(t) = \sqrt{\frac{\phi^2}{2}}\,(x_c + x_c\psi_0)\,, \tag{9}$$

and the complementary error function is given by $\mathrm{erfc}(x) = (2/\sqrt{\pi})\int_x^\infty \mathrm{d}z e^{-z^2}$.

The variation of $Q_c(t, x_c)$ as function of time t quantifies the fraction of transition-paths within the time period t, and so it can be identified as the PDF of the TPT, or simply, the transition-time density (TTD). Incorporating the normalisation constant, one can write the TTD as

$$\wp(t) = \frac{1}{Q_0(x_c)}\frac{\mathrm{d}}{\mathrm{d}t}Q_c(t, x_c) = -\frac{1}{Q_0(x_c)}\frac{1}{\sqrt{\pi}}\frac{\mathrm{d}q(t)}{\mathrm{d}t}e^{-q^2(t)}, \tag{10}$$

where the long-time limit of $Q_c(t, x_c)$ can be expressed as

$$Q_0(x_c) = \lim_{t\to\infty} Q_c(t, x_c) = \int_{x_c}^\infty \mathrm{d}x_t \lim_{t\to\infty} P(x_t, t|-x_c, 0). \tag{11}$$

In the long-time limit in comparison to both persistence and damping times, i.e. for $t \gg \tau_A$ and $t \gg 1/\gamma$, one can calculate (11) (for details see appendix C), yielding

$$Q_0(x_c) = \int_{x_c}^\infty \mathrm{d}x_t \lim_{t\to\infty} P(x_t, t|-x_c, 0) \approx \frac{1}{2}\mathrm{erfc}\sqrt{\epsilon_A}, \tag{12}$$

where the scaled (effective) energy barrier for the active case is given by

$$\epsilon_A = \frac{(\lambda+\gamma)^2 x_c^2}{16\left(\frac{\Delta}{2}^2 + \frac{\gamma^2 D_\mathrm{T}}{\lambda-\gamma} + \frac{2\gamma^2 D_A}{(\lambda-\gamma)(\tau_A(\lambda-\gamma)+2)}\right)}. \tag{13}$$

Figure 1 shows the TTD for different strengths and persistence times of the active noise as well as the friction coefficient of the medium, keeping the mass of the particle constant. The behaviour of the TTD is determined by the term $\exp(-q^2(t))$ at short times. From equation (C.6) it is clear that $q^2(t)$ diverges at a short times and, consequently, the TTD converges to zero, as shown in figure 1. The time scale depends on σ_0 (or σ_m), τ_A, and γ. Since $q^2(t)$ is directly proportional to γ^2 at fixed temperature (see equation (C.6)), and $q^2(t) \propto 1/\sigma_0^2$, the TTD vanishes comparatively at a larger rate in the low-friction limit and for higher values of the active force σ_0 or σ_m. At intermediate times the TTD attains a peak at $t = \tau_m$, corresponding to the most probable TPT. The peak shifts towards shorter times as σ_0 (or σ_m) increases and γ decreases, as illustrated in figure 1. Although the dependence of the active diffusivity as well as the friction coefficient on the TTD is similar in both models, the persistence time τ_A has different effects in the two cases. Let us first consider the intermediate and high-friction limits when $\gamma > 1$. Here τ_m takes higher values for higher τ_A in the OUP case, while the reverse trend with insignificant differences in τ_m can be observed in the MOU process, as shown in panels (b) and (d) of figure 1. In the underdamped regime, when $\gamma < 1$ the TTD for the former case follows a similar behaviour as in the previous limits. But in the case of the MOU process, τ_m varies with τ_A in a different manner: it shifts towards lower values in the small τ_A limit while it increases with τ_A in the opposite limit. So there exists a nonmonotonic variation of τ_m, hinting at the existence of an optimal transition rate. The TTD at longer times reaches asymptotically (see equation (C.5))

$$\lim_{t\to\infty}\wp(t) \sim \frac{2\sqrt{\epsilon_A}}{\mathrm{erfc}\sqrt{\epsilon_A}}\frac{e^{-\epsilon_A}}{\sqrt{\pi}}\frac{\lambda(\lambda-\gamma)}{(\lambda+\gamma)}e^{-\frac{\lambda}{2}t+\frac{\gamma}{2}t}, \tag{14}$$

for $\epsilon_A \gg 1$. Thus the leading-order behaviour is $\wp(t) \sim \epsilon_A e^{-\frac{\lambda}{2}t+\frac{\gamma}{2}t}$, confirming an exponential tail in the long-time limit. With increasing D_A, ϵ_A takes lower values and, therefore, the exponential tail of the TTD decays faster for a system with higher active diffusivity. A similar argument can be presented to justify the dependence of τ_A on the TTD, as shown in panels (b) and (d) of figure 1. In the high-friction limit, $\wp(t) \simeq e^{-\frac{\kappa_b}{m\gamma}t}$, suggesting that the exponential function decays slowly with γ, as can be understood from figure 1.

The mean TPT corresponds to the first moment of the TTD,

$$\langle t_\mathrm{TP}\rangle = \int_0^\infty \mathrm{d}t' t' \wp(t'). \tag{15}$$

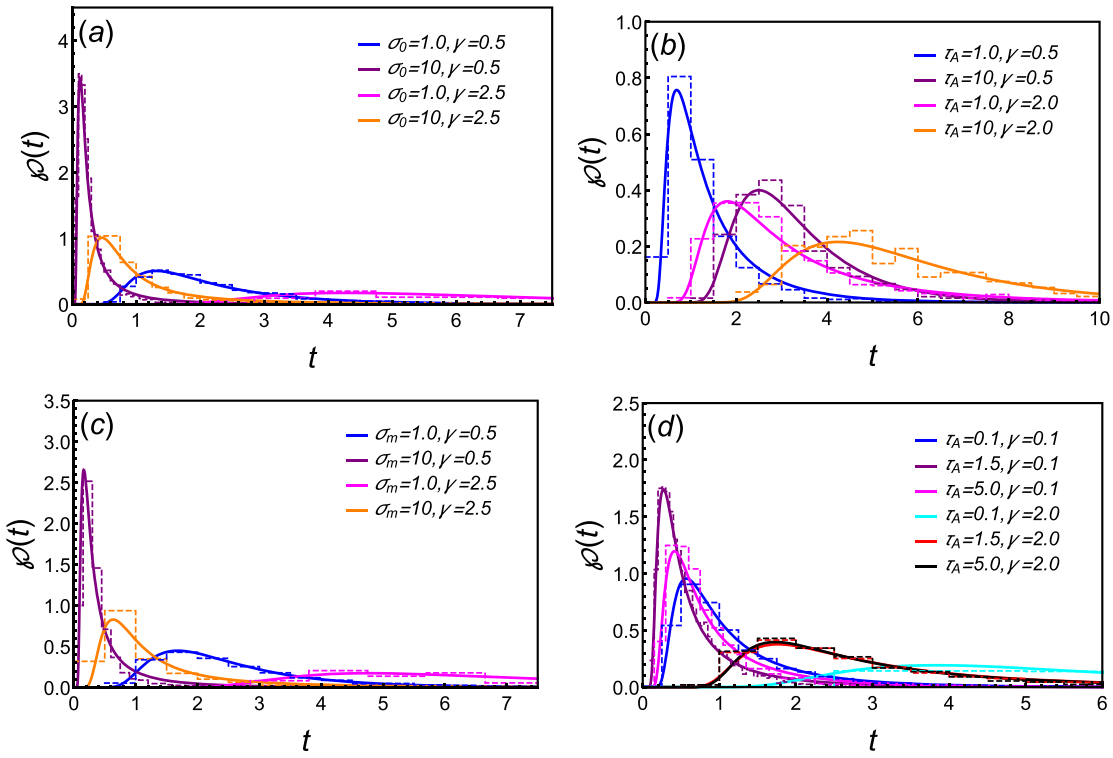

Figure 1. Transition-time density (TTD) versus time for two models of active noise, (a)–(b) the OU process, and (c)–(d) the MOU process. The simulation results shown by the dashed histograms are in good agreement with the theoretical densities of equation (10) (solid lines). The simulation details are provided in appendix B. In panels (a) and (c), the variations of the TTD are shown for different values of the correlation strengths of the active forces and the friction coefficient γ, for $\tau_A = 0.5$ and $\tau_A = 1.0$, respectively. For both models, we take $x_c = 1$ and $T = 0.01$. Other parameters are taken as unity. In panels (b) and (d), the correlation strengths of the active forces are set to $\sigma_0 = 2.5$ and $\sigma_m = 2.5$, respectively. Other parameters are $T = 0.01$, $m = 1$, $x_c = 1$, and $\kappa_b = \kappa_w = 1$.

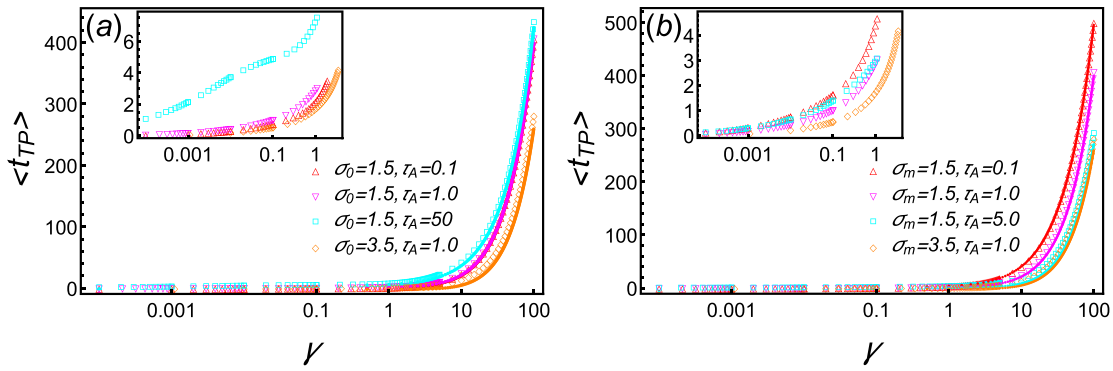

Figure 2. Log-linear plot of the mean transition-path time as function of the friction coefficient γ for two models of active noise: (a) the OU process and (b) the MOU process. The curves with symbols are obtained from numerical integration of equation (15), and they are in good agreement with the approximate result (16) represented by the solid lines in the moderate to high friction limits. In the insets, the plots are enlarged to highlight the underdamped regime. Other parameters used here are $T = 0.01$, $m = 1$, $x_c = 1$, $\kappa_b = 1$, $\kappa_w = 1$, and $k_B = 1$.

For high barriers, $\epsilon_A \gg 1$, the mean TPT can be approximated as (see equation (D.3))

$$\langle t_{TP} \rangle \approx \frac{2}{\lambda - \gamma} \ln\left(\frac{4\lambda e^{\gamma_e}}{\lambda + \gamma}\right) + \frac{2}{\lambda - \gamma} \ln(\epsilon_A) + \mathcal{O}\left(\frac{1}{\epsilon_A}\right), \tag{16}$$

where $\gamma_e \approx 0.577\,216$ is the Euler–Mascheroni constant. Figure 2 shows results from numerical integration of equation (15). The approximate result (16) agrees well with the numerical evaluation of the full expression. Notice that the mean TPT scales with ϵ_A logarithmically for both the passive and active cases. However, as we already mentioned that $\epsilon_p > \epsilon_A$, the mean TPT $\langle t_{TP} \rangle$ for the active case is lower as compared to the passive case. Thus an active particle needs, on average, comparatively less time for the effective barrier crossing. In

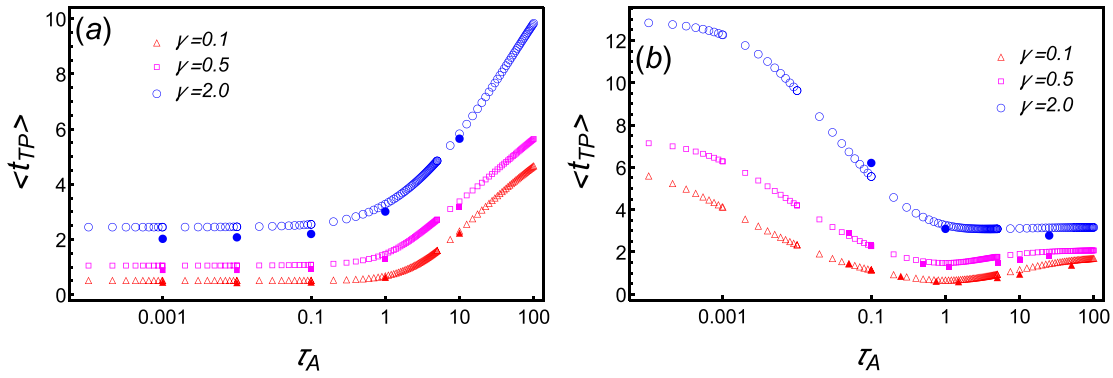

Figure 3. Log-linear plots of the mean transition-path time as function of the persistence time τ_A of the active noise for the two models: (a) the OU process and (b) the MOU process. The curves with open symbols are obtained from numerical integration of equation (15), they compare nicely with the simulations results represented by filled symbols. Other parameters used here are $\sigma_0 = 2.5$, $\sigma_m = 2.5$, $T = 0.01$, $m = 1$, $x_c = 1$, $\kappa_b = 1$, $\kappa_w = 1$, and $k_B = 1$.

the high-friction limit, $\langle t_{TP}\rangle \approx (m\gamma)/(\kappa_b)\ln(2e^{\gamma_e}\epsilon_A)$, which means that the mean TPT increases linearly with the friction coefficient, as depicted in figure 2. This is obvious as the dynamics gets slowed down in the presence of large friction, and thus it becomes more difficult for the particle to overcome the energy barrier. For $\gamma \to 0$, $\langle t_{TP}\rangle \approx \sqrt{m/\kappa_b}\ln(4e^{\gamma_e}\epsilon_A)$, which is independent of γ. But this limiting case does only exist if the particle gets enough time to attain the steady state within the well, i.e. for $\gamma\epsilon_A \gg \sqrt{\kappa_w/\gamma}$.

The insets of figures 2(a) and (b) show the variation of the TPT for different values of τ_A in the underdamped regime, and the trend is very similar to that of τ_m. To get a good an idea about this behaviour, we compute the TPTs from direct numerical simulation, which are then compared with the ones obtained from equation (15): the results of both methods are in good agreement. The TPT is plotted as a function of τ_A for three different values of the friction coefficient, as shown in figure 3. Let us first consider the OUP case, in which the effect of the persistence time τ_A is more prominent than the (effective) inertia in determining the dynamical properties [97]. For any value of γ, the TPT increases with τ_A, particularly at a significant rate in the high τ_A limit. The reason is that the correlation strength given by $\frac{\sigma_0^2}{\tau_A}$ (see equation (3)) decreases substantially with τ_A, thus hindering a directed trajectory to be successful in crossing the barrier. Let us now discuss the results of the model in which the active noise is characterised by the MOU process (see equation (5)). In order to explain the findings depicted in figure 3(b), one should consider two opposing mechanisms: randomisation and persistence. In the overdamped limit ($\gamma > 1$), very few transitions are expected to occur, and the rate will be faster if it is aided by a longer persistence of the motion. On the other hand, there are more frequent transitions in the underdamped limit ($\gamma < 1$), and so the competition between these opposing mechanisms is a vital factor. In the low τ_A limit, the particles get easily randomised, effecting an equilibrium-like situation, which can be characterised by an effective temperature $T_{\rm eff}$. With τ_A, the value of $T_{\rm eff}$ increases, thus scaling the effective energy barrier to lower values. So the transitions are faster and the TPT decreases until it reaches a point at which the randomisation process starts to be disturbed by longer persistent motion. Therefore, with further increase of τ_A, the particle gets oriented in specific directions. This causes easier transitions only for those particles oriented in the forward direction while making it even worse for the others to escape. So for a highly persistent, underdamped motion, the TPT increases with τ_A, as shown in figure 3(b). Such nonmonotonic variation of TPT is reminiscent of Kramers turnover, a well-known behaviour in chemical dynamics of passive systems. We note that such a turnover was recently found for levitated nanoparticles [104]. All these results for the TPT are consistent with the previous analyses presented in figures 1 and 2.

4. Conclusion

We studied the transition-path properties of a particle crossing a parabolic energy barrier in the presence of an exponentially correlated noise, modelled as OUP as well as MOUP process. In contrast to the previous study in [27] we here explicitly consider the underdamped dynamics and include the inertia of the particle as an effective parameter for the reduced description of a biomolecular reaction. Particularly, this effect was shown to become relevant when the dynamics is non-Markovian [81]. At moderate and high friction limits, the TPT is reduced with decreasing friction coefficient, which indirectly suggests that the underdamped dynamics facilitates effective crossings over the barrier. The shape of the transition-path distribution (TTD) remains exponential at long times for the active system, but the TTD shifts towards shorter time scales.

Similar to the passive case [34, 105], we also found that the TPT scales logarithmically with the effective energy barrier. However, in the presence of active noise, the effective diffusivity ($D_{\rm eff}$) is higher as compared to the passive case, and therefore the particle experiences a lower energy barrier ϵ_A, leading to shorter TPTs. Apart from the active diffusivity D_A, ϵ_A also depends on the persistence time τ_A and the stiffness of the well. In the OUP-noise case, the TPT increases monotonically with τ_A for any value of γ, although the increment is significantly higher in the overdamped limit, as has been found previously in [27]. Its behaviour is quite interesting in the MOUP case, namely, the TPT decreases as a function of τ_A in the overdamped limit while it shows a nonmonotonic variation in the underdamped regime ($\gamma < 1$), which is resultant of two competing processes: (i) rapid randomisation in the short τ_A limit and (ii) longer persistence due to higher values of τ_A. A very similar observations was found in [94] for an ABP in the underdamped limit In conclusion, we showed that without inertia the TPT is determined by the effective temperature. Taking the underdamped effects into consideration, and for a model where the interplay between inertial time and persistence time is important (e.g. in the MOUP case), two dynamical situations with two different escape kinetics emerge at two opposite limits of τ_A, and, therefore, a behaviour similar to the Kramers turnover is observed in an active system. One may employ our model in describing transition-path properties of activation-barrier limited biomolecular reactions occurring at non-equilibrium conditions. In future, it may be further extended to incorporate an asymmetric energy barrier instead of the symmetric parabolic shape used here, or to include the ruggedness of the potential landscape [12, 106–108].

Data availability statement

No new data were created in this study.

Appendix A. Derivation of the PDF with free boundary conditions

To get the propagator for the dynamics, we employ the phase-space path integral technique. In this formalism, one starts with the characteristic functional of the zero-mean white Gaussian noise $\eta(t)$ [109, 110],

$$\left\langle \exp\left(i\int_0^t {\rm d}t_1 p(t_1)\eta(t_1)\right)\right\rangle_\eta = \exp\left(-D_{\rm T}\int_0^t {\rm d}t_1 p^2(t_1)\right). \tag{A.1}$$

Taking the inverse Fourier transformation and mapping it to position space we can express the probability functional as [61]

$$\begin{aligned} P[x] = \int \exp\left(-D_{\rm T}\int_0^t {\rm d}t_1 p^2(t_1)\right) \exp\left(-i\int_0^t {\rm d}t_1 p(t_1)\left[\frac{1}{\gamma}\ddot{x}(t)+\dot{x}(t)-\frac{\kappa_b}{m\gamma}x(t)\right]\right) \\ \times\left\langle \exp\left(-i\int_0^t {\rm d}t_1 p(t_1)\sigma(t_1)\right)\right\rangle_\sigma \mathcal{D}p, \end{aligned} \tag{A.2}$$

where equation (6) has been used, and the angular bracket $\langle\cdot\rangle_\sigma$ denotes the average over all possible trajectories of the noise $\sigma(t)$. After some mathematical calculations, the above equation can be rewritten as

$$\begin{aligned} P[x] = \int \exp\left(-D_{\rm T}\int_0^t {\rm d}t_1 p^2(t_1)\right) \\ \times \exp\left(-i\frac{1}{\gamma}p_t v_t + i\frac{1}{\gamma}p_0 v_0 + i\frac{1}{\gamma}\dot{p}_t x_t - i\frac{1}{\gamma}\dot{p}_0 x_0 - ip_t x_t + ip_0 x_0\right) \\ \times \exp\left(-i\int_0^t {\rm d}t_1 x(t_1)\left[\frac{1}{\gamma}\ddot{p}(t_1)-\dot{p}(t_1)-\frac{\kappa_b}{m\gamma}p(t_1)\right]\right) \\ \times\left\langle \exp\left(-i\int_0^t {\rm d}t_1 p(t_1)\sigma(t_1)\right)\right\rangle_\sigma \mathcal{D}p, \end{aligned} \tag{A.3}$$

where $x(t) = x_t$, $x(0) = x_0$, $\dot{x}(t) = v_t$, and $\dot{x}(0) = v_0$. Therefore, the PDF to find the particle at position x_t with velocity v_t after time t, conditioned that it starts at position x_0 with velocity v_0, can be expressed as

$$P(x_t,v_t,t|x_0,v_0,t=0)=\int_{x(0)=x_0,\dot{x}(0)=v_0}^{x(t)=x_t,\dot{x}(t)=v_t}P[x]\mathcal{D}x$$
$$=\int\exp\left(-D_{\rm T}\int_0^t{\rm d}t_1p^2(t_1)\right)$$
$$\times\exp\left(-i\frac{1}{\gamma}p_tv_t+i\frac{1}{\gamma}p_0v_0+i\frac{1}{\gamma}\dot{p}_tx_t-i\frac{1}{\gamma}\dot{p}_0x_0-ip_tx_t+ip_0x_0\right)$$
$$\times\left\langle\exp\left(-i\int_0^t{\rm d}t_1p(t_1)\sigma(t_1)\right)\right\rangle_\sigma\mathcal{D}p$$
$$\times\int_{x(0)=x_0,\dot{x}(0)=v_0}^{x(t)=x_t,\dot{x}(t)=v_t}\exp\left(-i\int_0^t{\rm d}t_1x(t_1)\left[\frac{1}{\gamma}\ddot{p}(t_1)-\dot{p}(t_1)-\frac{\kappa_b}{m\gamma}p(t_1)\right]\right)\mathcal{D}x. \quad (A.4)$$

The path integration over x can be performed easily, as it leads to the delta functional

$$\delta\left(\frac{1}{\gamma}\ddot{p}(t_1)-\dot{p}(t_1)-\frac{\kappa_b}{m\gamma}p(t_1)\right). \quad (A.5)$$

This implies

$$p(t_1)=\frac{1}{\exp(\lambda t)-1}\left[p_0\left(\exp\left(\frac{1}{2}t_1(\gamma-\lambda)+\lambda t\right)-\exp\left(\frac{1}{2}t_1(\gamma+\lambda)\right)\right)\right.$$
$$\left.+p_t\left(\exp\left(\frac{1}{2}\left(t(\lambda-\gamma)+t_1(\gamma+\lambda)\right)\right)-\exp\left(\frac{1}{2}\left(t_1-t\right)(\gamma-\lambda)\right)\right)\right] \quad (A.6)$$

where $\lambda=\gamma\sqrt{1+4\kappa_b/(m\gamma^2)}$. Using the values of $p(t)$, equation (A.4) can further be simplified to

$$P(x_t,v_t,t|x_0,v_0,t=0)=\frac{1}{2\pi}\int{\rm d}p_t\int{\rm d}p_0\left\langle\exp\left(-i\int_0^t{\rm d}t_1p(t_1)\sigma(t_1)\right)\right\rangle_\sigma$$
$$\times\exp\left(-D_{\rm T}\int_0^t{\rm d}t_1p^2(t_1)\right)$$
$$\times\exp\left(-i\frac{1}{\gamma}p_tv_t+i\frac{1}{\gamma}p_0v_0+i\frac{1}{\gamma}\dot{p}_tx_t-i\frac{1}{\gamma}\dot{p}_0x_0-ip_tx_t+ip_0x_0\right). \quad (A.7)$$

The particle reaches the final exit point with a distributed velocity v_t. Thus we should integrate the propagator over all values of v_t, i.e.

$$P(x_t,t|x_0,v_0,t=0)=\int_{-\infty}^{\infty}{\rm d}v_tP(x_t,v_t,t|x_0,v_0,t=0)$$
$$=\frac{1}{2\pi}\int{\rm d}p_t\int{\rm d}p_0\exp\left(-D_{\rm T}\int_0^t{\rm d}t_1p^2(t_1)\right)\left\langle\exp\left(-i\int_0^t{\rm d}t_1p(t_1)\sigma(t_1)\right)\right\rangle_\sigma$$
$$\times\int_{-\infty}^{\infty}{\rm d}v_t\exp\left(-i\frac{1}{\gamma}p_tv_t+i\frac{1}{\gamma}p_0v_0+i\frac{1}{\gamma}\dot{p}_tx_t-i\frac{1}{\gamma}\dot{p}_0x_0-ip_tx_t+ip_0x_0\right)$$
$$=\frac{1}{2\pi}\int{\rm d}p_t\int{\rm d}p_0\exp\left(-D_{\rm T}\int_0^t{\rm d}t_1p^2(t_1)\right)\delta\left(\frac{1}{\gamma}p_t\right)\left\langle\exp\left(-i\int_0^t{\rm d}t_1p(t_1)\sigma(t_1)\right)\right\rangle_\sigma$$
$$\times\exp\left(i\frac{1}{\gamma}p_0v_0+i\frac{1}{\gamma}\dot{p}_tx_t-i\frac{1}{\gamma}\dot{p}_0x_0-ip_tx_t+ip_0x_0\right)$$
$$=\int\frac{{\rm d}p_0}{2\pi}\exp\left(-D_{\rm T}\int_0^t{\rm d}t_1p^2(t_1)\right)\exp\left(i\frac{1}{\gamma}p_0v_0+i\frac{1}{\gamma}\dot{p}_tx_t-i\frac{1}{\gamma}\dot{p}_0x_0+ip_0x_0\right)$$
$$\times\left\langle\exp\left(-i\int_0^t{\rm d}t_1p(t_1)\sigma(t_1)\right)\right\rangle_\sigma, \quad (A.8)$$

where $p(t_1)=p_0\exp\left(\frac{\gamma t_1}{2}\right)\sinh\left(\frac{\lambda}{2}(t-t_1)\right)/\sinh\left(\frac{\lambda}{2}t\right)$, as $p_t=0$.

As mentioned earlier, the particle is at a non-equilibrium steady state inside the left well at time $t=0$. We assume the potential of the well as harmonic, of the specific form $V_{\rm w}(x)=\frac{1}{2}\kappa_{\rm w}(x+x_{\rm w})^2$, where $\kappa_{\rm w}$ and $x_{\rm w}$ are the stiffness of the well and the position of the minimum, respectively. Thus the velocity of the particle in the harmonic potential follows the Boltzmann distribution with an effective temperature (defined by the

kinetic energy) $T_{\rm eff}$, which is different from the ambient temperature $T = m\gamma D_{\rm T}/k_{\rm B}$. The distribution of the initial velocity v_0 is given by [97]

$$P(v_0) = \sqrt{\frac{1}{2\pi\Delta^2}}\exp\left(-\frac{v_0^2}{2\Delta^2}\right), \tag{A.9}$$

where $\Delta^2 = \gamma\left(D_{\rm T} + D_A/[1+\gamma\tau_A + \frac{\kappa_{\rm w}}{m}\tau_A^2]\right)$. The (unnormalised) propagator for the position can then be expressed as

$$\begin{aligned}
P(x_t,t|x_0,t=0) &= \int {\rm d}v_0\, P(x_t,t|x_0,v_0,t=0)P(v_0)\\
&= \frac{1}{2\pi}\sqrt{\frac{1}{2\pi\Delta^2}}\int {\rm d}v_0\int {\rm d}p_0 \exp\left(-\frac{v_0^2}{2\Delta^2}\right)\exp\left(-D_{\rm T}\int_0^t {\rm d}t_1 p^2(t_1)\right)\\
&\quad\times\left\langle \exp\left(-i\int_0^t {\rm d}t_1 p(t_1)\sigma(t_1)\right)\right\rangle_\sigma \exp\left(\frac{i}{\gamma}p_0v_0 + \frac{i}{\gamma}\dot{p}_t x_t - \frac{i}{\gamma}\dot{p}_0x_0 + ip_0x_0\right)\\
&= \int\frac{{\rm d}p_0}{2\pi}\exp\left(-D_{\rm T}p_0^2\int_0^t {\rm d}t_1 e^{\gamma t_1}\frac{\sinh^2\left(\frac{\lambda}{2}(t-t_1)\right)}{\sinh^2\left(\frac{\lambda}{2}t\right)} - \frac{\Delta^2}{2\gamma^2}p_0^2 + \frac{i}{\gamma}\dot{p}_t x_t - \frac{i}{\gamma}\dot{p}_0x_0 + ip_0x_0\right)\\
&\quad\times\exp\left(-\frac{D_A}{2\tau_A}\int_0^t {\rm d}t_1\int_0^t {\rm d}t_2 p(t_1)\exp\left(-\frac{|t_1-t_2|}{\tau_A}\right)p(t_2)\right).
\end{aligned} \tag{A.10}$$

Note that the propagator must satisfy the normalisation condition $\int {\rm d}x_t P(x_t,t|x_0=-x_c,t=0)=1$. Therefore, from the above equation, one can find that the normalisation constant is $\sqrt{\phi_1^2/(4\gamma^2)}$, where $\phi_1^2 = \lambda^2 e^{\gamma t}/\sinh^2(\lambda t/2)$. Using this constant, we write the normalised propagator as

$$P(x_t,t|x_0,t=0) = \sqrt{\frac{\phi^2}{2\pi}}\exp\left(-\frac{\phi^2}{2}\left(x_t - x_0\psi_0\right)^2\right), \tag{A.11}$$

where the average position is

$$\psi_0(t) = e^{-\gamma t/2}\cosh\left(\frac{\lambda t}{2}\right) + \frac{\gamma}{\lambda}e^{-\gamma t/2}\sinh\left(\frac{\lambda t}{2}\right), \tag{A.12}$$

and the variance of the position is

$$\phi^2(t) = \left(\frac{\phi_1}{\phi_2}\right)^2. \tag{A.13}$$

Here we used the additional abbreviation

$$\begin{aligned}
\phi_2^2 &= 4\Delta^2 + \frac{4\gamma D_{\rm T}\left(-2\gamma^2 - \lambda{\rm csch}^2\left(\lambda t/2\right)\left[\lambda - \lambda e^{\gamma t} + \gamma\sinh(\lambda t)\right]\right)}{(\gamma-\lambda)(\gamma+\lambda)}\\
&\quad + 8\frac{\gamma D_A{\rm csch}^2\left(\frac{\lambda t}{2}\right)}{\left[(\gamma-\lambda)(\gamma+\lambda)\left(\tau_A(\gamma-\lambda)+2\right)\left(\tau_A(\lambda-\gamma)+2\right)\left(\tau_A(\gamma+\lambda)-2\right)\left(\tau_A(\gamma+\lambda)+2\right)\right]}\\
&\quad\times\Big[(\gamma-\lambda)(\gamma+\lambda)\left(\gamma\tau_A-2\right) + 2\lambda^2 e^{\gamma t}\left(\gamma\tau_A+1\right)\left(-\gamma\tau_A+\lambda\tau_A+2\right)\left(\tau_A(\gamma+\lambda)-2\right)\\
&\quad\times\left(\gamma\tau_A-\lambda\tau_A+2\right)\left(\tau_A(\gamma+\lambda)+2\right) + 4\gamma\lambda\tau_A^2(\gamma-\lambda)(\gamma+\lambda)e^{\frac{1}{2}t\left(\gamma-\frac{2}{\tau_A}\right)}\\
&\quad\times\left(\left(\gamma\tau_A+2\right)\sinh\left(\frac{\lambda t}{2}\right) + \lambda\tau_A\cosh\left(\frac{\lambda t}{2}\right)\right) - \gamma\left(\gamma\tau_A-\lambda\tau_A+2\right)\left(\tau_A(\gamma+\lambda)+2\right)\\
&\quad\times\left[\left(\tau_A\left(\gamma^2+\lambda^2\right)-2\gamma\right)\cosh(\lambda t) + 2\lambda(\gamma\tau_A-1)\sinh(\lambda t)\right]\Big].
\end{aligned} \tag{A.14}$$

Appendix B. Numerical method for the computation of $\wp(t)$

Numerical simulations of equation (6) are performed employing the Euler–Maruyama algorithm for 10^4 particles with time-step ${\rm d}t = 10^{-3}$, and the trajectories of active noise are generated using the discretised version of equations (2) and (4) for the OU and MOU processes, respectively. The particles are initially at

position $-x_c$ and are allowed to evolve in the inverted parabolic potential $V(x) = -\frac{k_b}{2}x^2$ according to equation (6). The initial velocities are chosen from the steady-state distribution given in (A.9), and for each particle, the active force is initially sampled from the normal distribution with zero mean and variance $\frac{D_A}{\tau_A}$ for the OUP case (and variance D_A for the MOUP case). While the particle is in the region $x < -x_c$, it is discarded as a no-transition event. When a particle crosses the point $x_c = +1$ (absorbing boundary) it is counted as a transition event, and the time is recorded as the TPT. The time data are represented as the histogram shown in figure 1. Note that here we only consider the forward rate, i.e. the rate of transition from $-x_c$ to $+x_c$, as the reverse rate may differ due to the imposition of a nonequilibrium condition.

Appendix C. Limiting values of $q(t)$ and ε_A

We first consider two limiting cases for $q(t)$, given by equation (9). In the long-time limit, i.e. for $\gamma t \gg 1$ and $\lambda t \gg 1$, one gets

$$\psi_0 \sim \frac{\lambda+\gamma}{2\lambda} e^{-\gamma t/2+\lambda t/2}\left[1+\frac{\lambda-\gamma}{\lambda+\gamma}e^{-\lambda t}\right], \tag{C.1}$$

$$\phi_1^2 \sim 4\lambda^2 e^{\gamma t-\lambda t}, \tag{C.2}$$

$$\phi_2^2 \sim 4\Delta^2 + \frac{8\gamma^2 D_{\mathrm{T}}}{\lambda-\gamma} + \frac{16\gamma^2 D_A}{(\lambda-\gamma)\left(\tau_A(\lambda-\gamma)+2\right)} \tag{C.3}$$

$$\phi^2 \sim \frac{\phi_1^2}{\phi_2^2} \sim \frac{4\lambda^2 e^{\gamma t-\lambda t}}{4\Delta^2 + \frac{8\gamma^2 D_{\mathrm{T}}}{\lambda-\gamma} + \frac{16\gamma^2 D_A}{(\lambda-\gamma)(\tau_A(\lambda-\gamma)+2)}}. \tag{C.4}$$

Thus $q(t)$ has the asymptotic limit

$$q^2(t) = \frac{\phi^2}{2}\left(x_c + x_c\psi_0\right)^2 \sim \epsilon_A\left[1+\frac{2\lambda}{\lambda+\gamma}e^{-\frac{\lambda}{2}t+\frac{\gamma}{2}t}\right]^2, \tag{C.5}$$

where ϵ_A is the barrier height divided by a modified (or effective) total energy as given by expression (13). For the passive case, $D_A \to 0$, and as a result, ϵ_A changes to $mx_c^2/(2k_{\mathrm{B}}T)$, which is denoted here as ϵ_p. Notice that $\epsilon_p > \epsilon_A$, and ϵ_A decreases with D_A as $\epsilon_A \propto 1/D_A$. From equation (12) we infer that $Q_0(x_c)_{\text{active}} > Q_0(x_c)_{\text{passive}}$, as illustrated in figure C1. This result is not surprising as the number of successful crossings increases with the help of the higher energy provided by the active fluctuations of the surroundings. With the increment of κ_b, the particle has to climb up a steeper (higher) energy barrier, and as a result, $Q_c(t, x_c)$ decreases. In the limit $\tau_A \to 0$, the correlation of the active (OUP) noise becomes a delta function and thus it can be thought of as a source of an extra thermal energy with active temperature $k_{\mathrm{B}}T_A = m\gamma D_A$. Consequently, ϵ_A is given by the barrier height divided by an effective thermal energy, i.e. $\epsilon_A = mx_c^2/[2k_{\mathrm{B}}(T+T_A)]$.

In the short-time limit $t \to 0$, one can approximate $q(t)$, yielding

$$q^2(t) \approx \frac{2x_c^2}{\gamma t^2}\frac{1}{D_{\mathrm{T}} + \frac{D_A}{1+\gamma\tau_A+\frac{\kappa_{\mathrm{W}}}{m}\tau_A^2}}. \tag{C.6}$$

For the passive case, $D_A \to 0$, and so $q^2(t)$ reduces to $q^2(t) \approx 2mx_c^2/(k_{\mathrm{B}}T)t^{-2}$, which is the same as the one obtained in [26]. At short times, the particle mostly stays near the minimum, which means that the contributions to the total energy mainly come from its motion, which exhibits short-time ballistic behaviour. For $q^2(t)$ in the active case, the energy is solely kinetic, like the passive case, but it is scaled by a relatively higher, supplied to the particle due to the presence of active fluctuations. Therefore, one has $q(t)_{\text{passive}} > q(t)_{\text{active}}$, which, by virtue of expression (8), immediately suggests that $Q_c(t)_{\text{passive}} < Q_c(t)_{\text{active}}$. This is depicted in figure C1. From equations (C.5) and (C.6), one can see that $q(t)$ varies between ∞ and $\sqrt{\epsilon_A}$ over the time interval $t \in (0, \infty)$. Similarly, one has $Q_c(t, x_c) \in (0, Q_0(x_c))$.

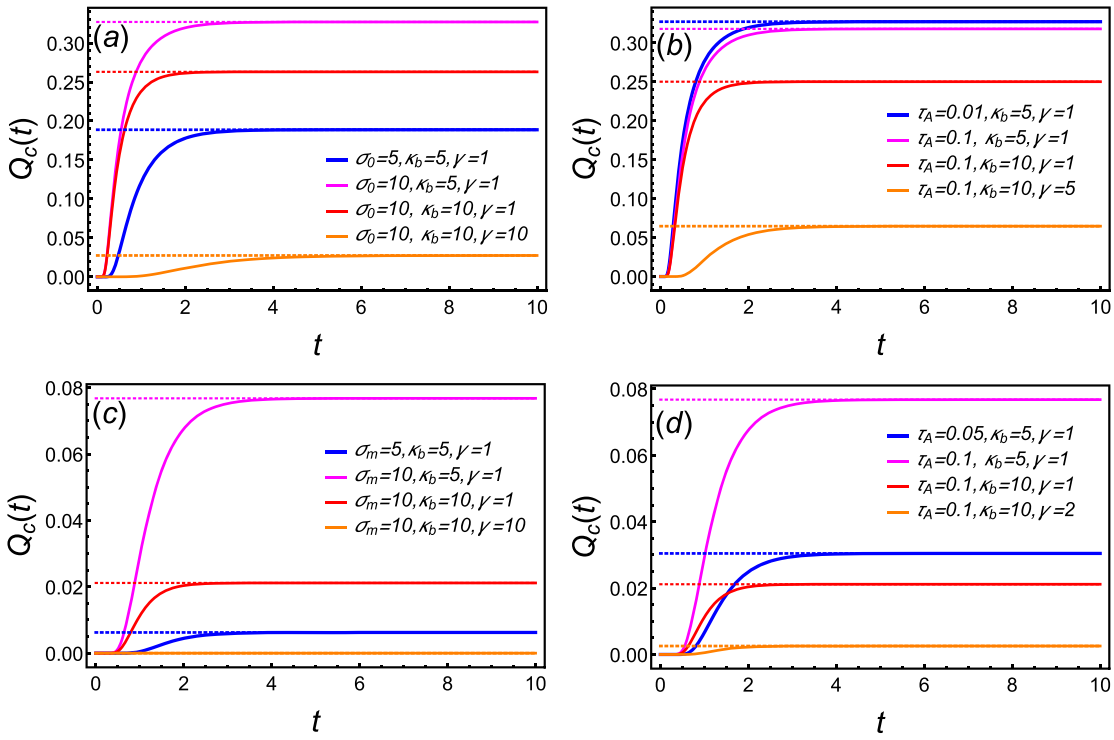

Figure C1. Absorption function (solid curves) as function of time for (a)–(b) the OUP-noise model and (c)–(d) the MOUP-noise model. In panels (a) and (c), the variation of $Q_c(t, x_c = 2)$ is shown for different values of the active forces (σ_0, σ_m), the friction coefficient γ, and the curvature κ_b of the potential around $x = 0$, for $\tau_A = 0.01$ and $\tau_A = 0.1$, respectively. The solid curves (equation (8)) in panels (b) and (d) correspond to different values of τ_A and κ_b, keeping $\sigma_0 = 10$ and $\sigma_m = 10$ fixed, respectively. The dashed lines correspond to the asymptotic values of the absorption function given by equation (12). Other parameters are taken as unity.

Appendix D. Approximation of $\langle t_{\rm TP}\rangle$

To obtain the average TPT in the high-energy barrier limit (i.e. for $\epsilon_A \gg 1$), we change the variable of integration in equation (15) from t to q, as demonstrated in [26]. Then the average TPT can be rewritten using equation (15), producing

$$\langle t_{\rm TP}\rangle = \int_0^\infty {\rm d}t' t' \wp(t') = \frac{\int_{\sqrt{\epsilon_A}}^\infty {\rm d}q t(q) e^{-q^2}}{\int_{\sqrt{\epsilon_A}}^\infty {\rm d}q e^{-q^2}} = \frac{\int_0^\infty {\rm d}x \frac{t(x)}{\sqrt{1+x/\epsilon_A}} e^{-x}}{\int_0^\infty {\rm d}x \frac{1}{\sqrt{1+x/\epsilon_A}} e^{-x}}. \tag{D.1}$$

In the last step we used $x = q^2 - \epsilon_A$. In the long-time limit, one can write the time t as a function of $q(t)$ using equation (C.5), resulting in

$$\begin{aligned} t &\approx \frac{2}{\lambda-\gamma}\ln\left(\frac{2\lambda}{\lambda+\gamma}\right) - \frac{2}{\lambda-\gamma}\ln\left(\frac{q(t)}{\sqrt{\epsilon_A}} - 1\right) \\ &\approx \frac{2}{\lambda-\gamma}\ln\left(\frac{2\lambda}{\lambda+\gamma}\right) - \frac{2}{\lambda-\gamma}\ln\left(\sqrt{1+x/\epsilon_A} - 1\right). \end{aligned} \tag{D.2}$$

Considering $\epsilon_A \gg 1$, we can perform the integration in equation (D.1), finding

$$\begin{aligned} \langle t_{\rm TP}\rangle &\approx \frac{2}{\lambda-\gamma}\ln\left(\frac{2\lambda}{\lambda+\gamma}\right) - \frac{2}{\lambda-\gamma}\int_0^\infty {\rm d}x \ln\left(\frac{x}{2\epsilon_A}\right) e^{-x} + \mathcal{O}\left(\frac{1}{\epsilon_A}\right) \\ &\approx \frac{2}{\lambda-\gamma}\ln\left(\frac{2\lambda}{\lambda+\gamma}\right) + \frac{2}{\lambda-\gamma}\ln 2 + \frac{2}{\lambda-\gamma}\gamma_e \\ &\quad + \frac{2}{\lambda-\gamma}\ln(\epsilon_A) + \mathcal{O}\left(\frac{1}{\epsilon_A}\right), \end{aligned} \tag{D.3}$$

where $\gamma_e = -\int_0^\infty {\rm d}x \ln(x)\, e^{-x} \approx 0.577\,216$ is the Euler–Mascheroni constant.

ORCID iDs

Koushik Goswami https://orcid.org/0000-0002-0632-9654
Ralf Metzler https://orcid.org/0000-0002-6013-7020

References

[1] Hänggi P, Talkner P and Borkovec M 1990 *Rev. Mod. Phys.* **62** 251
[2] Socci N D, Onuchic J N and Wolynes P G 1996 *J. Chem. Phys.* **104** 5860
[3] Wang J, Onuchic J and Wolynes P 1996 *Phys. Rev. Lett.* **76** 4861
[4] Woodside M T, Anthony P C, Behnke-Parks W M, Larizadeh K, Herschlag D and Block S M 2006 *Science* **314** 1001
[5] Volk M, Milanesi L, Waltho J P, Hunter C A and Beddard G S 2015 *Phys. Chem. Chem. Phys.* **17** 762
[6] Kramers H A 1940 *Physica* **7** 284
[7] Berezhkovskii A and Szabo A 2005 *J. Chem. Phys.* **122** 014503
[8] Nitzan A 2006 *Chemical Dynamics in Condensed Phases: Relaxation, Transfer and Reactions in Condensed Molecular Systems* (Oxford: Oxford University Press)
[9] Kirmizialtin S, Huang L and Makarov D E 2005 *J. Chem. Phys.* **122** 234915
[10] Best R B and Hummer G 2005 *Proc. Natl Acad. Sci. USA* **102** 6732
[11] Best R B and Hummer G 2006 *Phys. Rev. Lett.* **96** 228104
[12] Palyulin V V, Ala-Nissila T and Metzler R 2014 *Soft Matter* **10** 9016
[13] Hu X, Hong L, Dean Smith M, Neusius T, Cheng X and Smith J C 2016 *Nat. Phys.* **12** 171
[14] Yang H, Luo G, Karnchanaphanurach P, Louie T-M, Reich I, Cova S, Xun L and Xie X S 2003 *Science* **302** 262
[15] Yamamoto E, Akimoto T, Mitsutake A and Metzler R 2021 *Phys. Rev. Lett.* **126** 128101
[16] Kim P S and Baldwin R L 1990 *Annu. Rev. Biochem.* **59** 631
[17] Jacob M, Schindler T, Balbach J and Schmid F X 1997 *Proc. Natl Acad. Sci. USA* **94** 5622
[18] Chung H S, Louis J M and Eaton W A 2009 *Proc. Natl Acad. Sci. USA* **106** 11837
[19] Hummer G 2004 *J. Chem. Phys.* **120** 516
[20] Hummer G and Eaton W A 2012 *Physics* **5** 87
[21] Pollak E and Talkner P 2005 *Chaos* **15** 026116
[22] Li P C and Makarov D E 2003 *J. Chem. Phys.* **119** 9260
[23] Engel M C, Ritchie D B, Foster D A N, Beach K S D and Woodside M T 2014 *Phys. Rev. Lett.* **113** 238104
[24] Manuel A P, Lambert J and Woodside M T 2015 *Proc. Natl Acad. Sci. USA* **112** 7183
[25] Berezhkovskii A M, Hummer G and Bezrukov S M 2006 *Phys. Rev. Lett.* **97** 020601
[26] Laleman M, Carlon E and Orland H 2017 *J. Chem. Phys.* **147** 214103
[27] Carlon E, Orland H, Sakaue T and Vanderzande C 2018 *J. Phys. Chem.* B **122** 11186
[28] Medina E, Satija R and Makarov D E 2018 *J. Phys. Chem.* B **122** 11400
[29] Singh D, Mondal K and Chaudhury S 2021 *J. Phys. Chem.* B **125** 4536
[30] Piana S, Lindorff-Larsen K and Shaw D E 2012 *Proc. Natl Acad. Sci. USA* **109** 17845
[31] Piana S, Donchev A G, Robustelli P and Shaw D E 2015 *J. Phys. Chem.* B **119** 5113
[32] Avdoshenko S M, Das A, Satija R, Papoian G A and Makarov D E 2017 *Sci. Rep.* **7** 1
[33] Neupane K, Ritchie D B, Yu H, Foster D A N, Wang F and Woodside M T 2012 *Phys. Rev. Lett.* **109** 068102
[34] Chung H S, McHale K, Louis J M and Eaton W A 2012 *Science* **335** 981
[35] Pollak E 2016 *Phys. Chem. Chem. Phys.* **18** 28872
[36] Truex K, Chung H S, Louis J M and Eaton W A 2015 *Phys. Rev. Lett.* **115** 018101
[37] Neupane K, Foster D A N, Dee D R, Yu H, Wang F and Woodside M T 2016 *Science* **352** 239
[38] Neupane K, Wang F and Woodside M T 2017 *Proc. Natl Acad. Sci. USA* **114** 1329
[39] Hoffer N Q and Woodside M T 2019 *Curr. Opin. Chem. Biol.* **53** 68
[40] Vilk O, Aghion E, Nathan R, Toledo S, Metzler R and Assaf M 2022 *J. Phys. A: Math. Theor.* **55** 334004
[41] Krapf D, Lukat N, Marinari E, Metzler R, Oshanin G, Selhuber-Unkel C, Squarcini A, Stadler L, Weiss M and Xu X 2019 *Phys. Rev.* X **9** 011019
[42] Dudko O K, Hummer G and Szabo A 2008 *Proc. Natl Acad. Sci. USA* **105** 15755
[43] Berezhkovskii A M, Dagdug L and Bezrukov S M 2017 *J. Phys. Chem.* B **121** 5455
[44] Berezhkovskii A M and Makarov D E 2019 *J. Chem. Phys.* **151** 065102
[45] Orland H 2011 *J. Chem. Phys.* **134** 174114
[46] Li H, Xu Y, Li Y and Metzler R 2020 *Euro. Phys. J. Plus* **135** 1
[47] Li H, Xu Y, Metzler R and Kurths J 2020 *Chaos Solit. Fractals* **141** 110293
[48] Makarov D E 2015 *J. Chem. Phys.* **143** 194103
[49] Satija R and Makarov D E 2019 *J. Phys. Chem.* B **123** 802
[50] Janakiraman D 2018 *J. Phys. A: Math. Theor.* **51** 285001
[51] Dutta R and Pollak E 2021 *Phys. Chem. Chem. Phys.* **23** 23787
[52] Zwanzig R 2001 *Nonequilibrium Statistical Mechanics* (Oxford: Oxford University Press)
[53] Makarov D E 2021 *J. Phys. Chem.* B **125** 2467
[54] Satija R, Berezhkovskii A M and Makarov D E 2020 *Proc. Natl Acad. Sci. USA* **117** 27116
[55] Satija R, Das A and Makarov D E 2017 *J. Chem. Phys.* **147** 152707
[56] Mizuno D, Tardin C, Schmidt C F and MacKintosh F C 2007 *Science* **315** 370
[57] Maggi C, Paoluzzi M, Pellicciotta N, Lepore A, Angelani L and Di Leonardo R 2014 *Phys. Rev. Lett.* **113** 238303
[58] Bechinger C, Di Leonardo R, Löwen H, Reichhardt C, Volpe G and Volpe G 2016 *Rev. Mod. Phys.* **88** 045006
[59] Ramaswamy S 2017 *J. Stat. Mech.: Theory Exp.* **2017** 054002
[60] Fodor E, Nardini C, Cates M E, Tailleur J, Visco P and van Wijland F 2016 *Phys. Rev. Lett.* **117** 038103
[61] Goswami K and Sebastian K L 2019 *J. Stat. Mech.: Theory Exp.* **2019** 083501
[62] Kearns D B 2010 *Nat. Rev. Microbiol.* **8** 634
[63] Caspi A, Granek R and Elbaum M 2000 *Phys. Rev. Lett.* **85** 5655

[64] Toyota T, Head D A, Schmidt C F and Mizuno D 2011 *Soft Matter* **7** 3234
[65] Fakhri N, Wessel A D, Willms C, Pasquali M, Klopfenstein D R, MacKintosh F C and Schmidt C F 2014 *Science* **344** 1031
[66] Song M S, Moon H C, Jeon J-H and Park H Y 2018 *Nat. Commun.* **9** 344
[67] Cherstvy A G, Nagel O, Beta C and Metzler R 2018 *Phys. Chem. Chem. Phys.* **20** 23034
[68] Lemaitre E, Sokolov I M, Metzler R and Chechkin A V 2023 *New J. Phys.* **25** 013010
[69] Shin J, Cherstvy A G, Kim W K and Metzler R 2015 *New J. Phys.* **17** 113008
[70] Weber S C, Spakowitz A J and Theriot J A 2012 *Proc. Natl Acad. Sci.* **109** 7338
[71] Goswami K 2019 *Physica* A **525** 223
[72] Chaki S and Chakrabarti R 2020 *Soft Matter* **16** 7103
[73] Goswami K 2021 *Physica* A **566** 125609
[74] Tripathi P, Firouzbakht A, Gruebele M and Wanunu M 2022 *J. Phys. Chem. Lett.* **13** 5918
[75] Reverey J F, Jeon J-H, Bao H, Leippe M, Metzler R and Selhuber-Unkel C 2015 *Sci. Rep.* **5** 11690
[76] Mashaghi A, Kramer G, Lamb D C, Mayer M P and Tans S J 2014 *Chem. Rev.* **114** 660
[77] Kuznets-Speck B and Limmer D T 2021 *Proc. Natl Acad. Sci.* **118** e2020863118
[78] Muthukumar M 2001 *Phys. Rev. Lett.* **86** 3188
[79] Saintillan D, Shelley M J and Zidovska A 2018 *Proc. Natl Acad. Sci. USA* **115** 11442
[80] Goswami K, Chaki S and Chakrabarti R 2022 *J. Phys. A: Math. Theor.* **55** 423002
[81] Brünig F N, Daldrop J O and Netz R R 2022 *J. Phys. Chem.* B **126** 10295
[82] Ballard A J and Dellago C 2012 *J. Phys. Chem.* B **116** 13490
[83] Klotsa D 2019 *Soft Matter* **15** 8946
[84] Löwen H 2020 *J. Chem. Phys.* **152** 040901
[85] Pastor R W and Karplus M 1989 *J. Chem. Phys.* **91** 211
[86] Rosenberg R O, Berne B J and Chandler D 1980 *Chem. Phys. Lett.* **75** 162
[87] Gosztolai A and Barahona M 2020 *Commun. Phys.* **3** 1
[88] van den Broek B, Lomholt M A, Kalisch S M, Metzler R and Wuite G J 2008 *Proc. Natal Acad. Sci. USA* **105** 15738
[89] Wang J, Chen Y, Yu W and Luo K 2016 *J. Chem. Phys.* **144** 204702
[90] Woillez E, Zhao Y, Kafri Y, Lecomte V and Tailleur J 2019 *Phys. Rev. Lett.* **122** 258001
[91] Woillez E, Kafri Y and Gov N S 2020 *Phys. Rev. Lett.* **124** 118002
[92] Zanovello L, Caraglio M, Franosch T and Faccioli P 2021 *Phys. Rev. Lett.* **126** 018001
[93] Schneider E and Stark H 2019 *Europhys. Lett.* **127** 64003
[94] Militaru A, Innerbichler M, Frimmer M, Tebbenjohanns F, Novotny L and Dellago C 2021 *Nat. Commun.* **12** 2446
[95] Goswami K 2019 *Phys. Rev.* E **99** 012112
[96] Risken H 1996 *Fokker-Planck Equation The Fokker-Planck Equation* (Berlin: Springer) p 63
[97] Goswami K 2022 *Phys. Rev.* E **105** 044123
[98] Caprini L and Marini Bettolo Marconi U 2021 *J. Chem. Phys.* **154** 024902
[99] Goswami K and Chakrabarti R 2022 *Soft Matter* **18** 2332
[100] Nguyen G H P, Wittmann R and Löwen H 2022 *J. Phys. Condens. Matter* **34** 035101
[101] Um J, Song T and Jeon J-H 2019 *Front. Phys.* **7** 143
[102] Jackson S E and Fersht A R 1991 *Biochemistry* **30** 10428
[103] Zhang B W, Jasnow D and Zuckerman D M 2007 *J. Chem. Phys.* **126** 074504
[104] Rondin L, Gieseler J, Ricci F, Quidant R, Dellago C and Novotny L 2017 *Nat. Nanotechnol.* **12** 2017
[105] Chung H S and Gopich I V 2014 *Phys. Chem. Chem. Phys.* **16** 18644
[106] Mattos T G, Mejía-Monasterio C, Metzler R and Oshanin G 2012 *Phys. Rev.* E **86** 031143
[107] Wagner C and Kiefhaber T 1999 *Proc. Natl Acad. Sci. USA* **96** 6716
[108] Zwanzig R 1988 *Proc. Natl Acad. Sci. USA* **85** 2029
[109] Van Kampen N G 1991 *Stochastic Processes in Physics and Chemistry* (Amsterdam: North-Holland)
[110] Kamenev A 2011 *Field Theory of Non-Equilibrium Systems* (Cambridge: Cambridge University Press)